






Article

Relative Sea-Level Rise and Potential Submersion Risk for 2100 on 16 Coastal Plains of the Mediterranean Sea

Fabrizio Antonioli ^{1,2,*} , Giovanni De Falco ³, Valeria Lo Presti ⁴, Lorenzo Moretti ², Giovanni Scardino ⁵ , Marco Anzidei ⁶, Davide Bonaldo ⁷, Sandro Carniel ⁸, Gabriele Leoni ⁹, Stefano Furlani ¹⁰ , Antonella Marsico ⁵, Marcello Petitta ², Giovanni Randazzo ¹¹, Giovanni Scicchitano ¹²  and Giuseppe Mastronuzzi ⁵ 

¹ Istituto Nazionale di Geofisica e Vulcanologia, 00143 Rome, Italy

² ENEA, 40129 Bologna, 00123 Rome, Italy; lorenzo.moretti@enea.it (L.M.); marcello.petitta@enea.it (M.P.)

³ Institute of Anthropic Impacts and Sustainability in Marine Environment—IAS CNR, 09170 Oristano, Italy; giovanni.defalco@cnr.it

⁴ Studio Tecnico, 90142 Palermo, Italy; valeria.lopresti@gmail.com

⁵ Department of Earth and Geoenvironmental Sciences, University of Bari, 70125 Bari, Italy; giovanni.scardino@uniba.it (G.S.); antonella.marsico@uniba.it (A.M.); giuseppe.mastronuzzi@uniba.it (G.M.)

⁶ National Institute of Geophysics and Volcanology, 00143 Rome, Italy; marco.anzidei@ingv.it

⁷ National Research Council, Institute of Marine Sciences (CNR-ISMAR), 30122 Venice, Italy; davide.bonaldo@ve.ismar.cnr.it

⁸ National Research Council, Institute of Polar Science (CNR-ISP), 30122 Venice, Italy; sandro.carniel70@gmail.com

⁹ ISPRA, 00144 Roma, Italy; gabriele.leoni@isprambiente.it

¹⁰ Department of Mathematics and Geosciences, University of Trieste, 34125 Trieste, Italy; sfurlani@units.it

¹¹ Department of Mathematics, Physics and Geosciences, MIFT, University of Messina, 98166 Messina, Italy; grandazzo@unime.it

¹² Studio Geologi Associati TST, 95129 Catania, Italy; scicchitano@studiogeologitst.com

* Correspondence: fabrizioantonioli2@gmail.com

Received: 5 June 2020; Accepted: 29 July 2020; Published: 1 August 2020



Abstract: The coasts of the Mediterranean Sea are dynamic habitats in which human activities have been conducted for centuries and which feature micro-tidal environments with about 0.40 m of range. For this reason, human settlements are still concentrated along a narrow coastline strip, where any change in the sea level and coastal dynamics may impact anthropic activities. In the frame of the RITMARE and the Copernicus Projects, we analyzed light detection and ranging (LiDAR) and Copernicus Earth Observation data to provide estimates of potential marine submersion for 2100 for 16 small-sized coastal plains located in the Italian peninsula and four Mediterranean countries (France, Spain, Tunisia, Cyprus) all characterized by different geological, tectonic and morphological features. The objective of this multidisciplinary study is to provide the first maps of sea-level rise scenarios for 2100 for the IPCC RCP 8.5 and Rahmstorf (2007) projections for the above affected coastal zones, which are the locations of touristic resorts, railways, airports and heritage sites. On the basis of our model (eustatic projection for 2100, glaciohydrostasy values and tectonic vertical movement), we provide 16 high-definition submersion maps. We estimated a potential loss of land for the above areas of between about 148 km² (IPCC-RCP8.5 scenario) and 192 km² (Rahmstorf scenario), along a coastline length of about 400 km.

Keywords: Mediterranean Sea; coastal plains; relative sea-level rise; 2100; marine submersion

1. Introduction

Sea-level rise is one of the major consequences of climate change which affects global communities living along coasts. This phenomenon is due to planetary-scale processes that are contributing to the current sea-level trend. The main responsible factors are global warming, which is driving the melting of ice and the thermal expansion of the oceans and finally the geological vertical movements of the land along the coastal zones, which may accelerate (or decrease) the submersion of low-elevated coasts.

Instrumental and observational data show that over the past two centuries, the global sea level has risen at faster rates than in the last two millennia [1–3], with values up to 3.2 mm/year over the last decades [4–7]. Recently, Toimil et al. [8] delineated the requirements for a scientific approach for future projections of shoreline change, which should take into account changes in the mean sea level, storm surges, coastal erosion and other additional factors, with the aim of reducing uncertainty in shoreline change estimates.

This rise is exposing many coastal areas around the world to coastal hazards and marine flooding. Sea-level rise and storm surge has been the indirect cause of dramatic effects in conjunction with extreme storm surge events, such as in 1953 for the coast of Netherlands (1953) or more recently in New Jersey (2012, Hurricane Sandy), Louisiana (2015, Hurricane Katrina), Florida (2016, Hurricane Matthew), Louisiana and Texas (2017, Hurricane Harvey).

In the Mediterranean basin, the sea level is rising at 1.8 mm/year, as inferred from the analysis of tidal gauge data for the last century. In 2100, the sea level could be 500–1400 mm higher than today due to the melting of continental ice and thermal expansion/steric effects as a consequence of global warming.

In this scenario, the coastal low lands will be more prone to marine flooding during extreme sea events, threatening many highly populated areas of the Mediterranean coasts.

In the last two decades, many studies have focused on sea-level rise and its effects along the continental (i.e., Gornitz et al. [9] for New York; Walsh et al. [10] for Australia; Miller et al. [11], Ezer and Atkinson [12] for USA; Rehman et al. [13] for India) and insular coasts (i.e., Wadey et al. [14] for Maldives) highlighting the relevant exposure to coastal hazard for lowlands and small islands. These studies are relevant in the Mediterranean, where about 75% of the local population lives in coastal areas [15] and is therefore exposed to the multiple effects of sea-level rise. Although several studies have attempted to predict global sea-level rise for 2100 [2,16–20] or even until 2200 [21], only in a few cases have sea-level rise projections been used in combination with high-resolution digital terrain models (DTM) and with geological data to evaluate the geomorphological landscape changes at different time scales, to draw detailed maps of the expected coastal submersion. In the Mediterranean, many coasts are expected to be flooded as a consequence of sea-level rise, storm surge and tsunamis, as inferred from seismic, geodetic, geological and archaeological evidence ([22,23], www.savemedcoasts.eu [24]). In this region, rapid urbanization started after the middle of the 19th century, which led to the uncontrolled expansion of coastal settlements; these settlements are now exposed to increasing coastal hazards. In addition, the coasts, which are often characterized by cultural and natural heritage sites, host important urban and industrial installations and continuously growing tourist activities.

An integrated approach to the analysis of the impacts of climate change in coastal areas is crucial for a thorough projection of coastal hazards and for the identification of response strategies and priorities. To this end, in the frame of the RITMARE project [25], the Adriatic Sea (in the north-eastern Mediterranean, Figure 1) has been considered a test site for a multidisciplinary study on coastal vulnerability to sea-level rise and erosion. This activity, funded by the Italian Ministry of University and Research, provided a proof-of-concept for how different observational and numerical modelling tools can be combined in the characterization of the physical drivers of coastal processes in a changing climate perspective. As emerged from the outcomes of RITMARE, the spatial modulation of interplaying geological/sedimentological and meteo-oceanographic processes in such complex systems puts serious limitations on the applicability of global and regional climate change projections

for the assessment of the local features of coastal vulnerability. A typical example is given by the possible impacts of storm surge hazards and erosion in future scenarios. Notwithstanding a general tendency toward a weaker storminess at the Mediterranean scale, the increasing sea level is expected to supersede the decrease of sea state severity [26,27]. In addition, local intensifications of the wave climate are possible in response to the northbound migration of the Mediterranean cyclone tracks, contributing to the further enhancement of the potential coastal hazard in coastal regions [28].

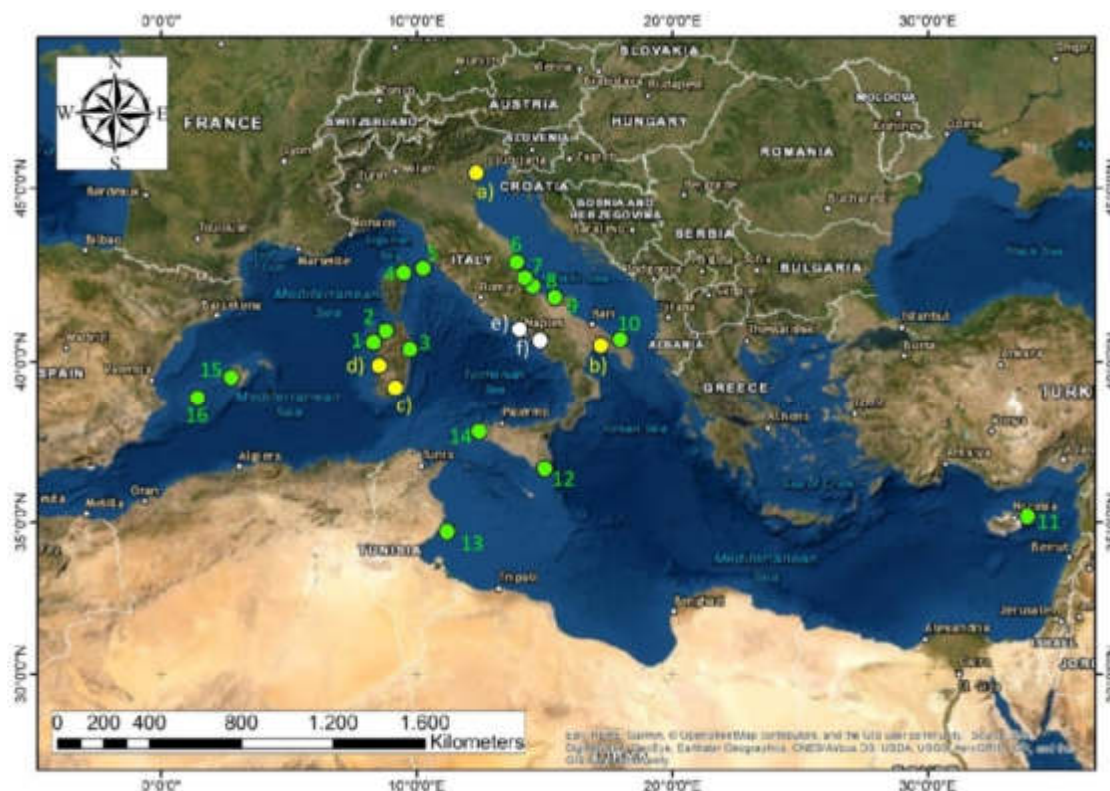


Figure 1. The Mediterranean coastal plains investigated in this paper (green dots) and previous studies by Antonioli et al. [29], Marsico et al. [30] (yellow marks and letters), Aucelli et al. [31,32] and Giordano et al. [33] (white marks and letters).

In the frame of the C3S European Tourism CLIMTOUR project (a sectorial climate service in the field of tourism which engages and interacts with a number of stakeholders across the six sectors of agriculture, tourism, insurance, coasts, infrastructure and health to establish an inventory of existing policy needs and user requirements in terms of climate data and climate impact indicators), researchers have been investigating the potential scenarios of sea-level rise in specific coasts of the Mediterranean European countries. Moreover, in the framework of the “Integrated Sea Storm Management Strategies” project (IWS, I-STORMS Web System; <https://iws.seastorms.eu> [34,35]) by the National Research Council of Italy Marine Sciences Institute (CNR-ISMAR), the Agency for Prevention, Environment and Energy of Emilia-Romagna, the Hydro-Meteo-Climatic Service (Arpae-SIMC), and Apulia Region Civil Protection, some other areas have been investigated along the coasts of Apulia in Southern Italy.

In this study, sea-level projections for 2100 estimated by the two global models IPCC-AR5 [36] and Rahmstorf [17] were used according to the method reported in Antonioli et al. [29] and Marsico et al. [30]. The proposed scenarios for the selected coastal plains include the contribution of vertical land movements (tectonics and isostasy) with rates based on the interpretation of geological data or modeling analysis. Our maps show the maximum sea-level height expected for 2100 for the above reference climatic projections and the corresponding flooded area. We remark that our analysis does not take into account hydrodynamics models, and the contribution of sediment flow from rivers, coastal erosion and possible anthropic defenses may change the estimated extension of the flooded

areas proposed in this study. This work provides additional scenarios with respect to previous studies [23,29,31,33,37–46] focusing on new areas which are at risk of marine submersion over the next decades.

2. Material and Method

This study is based on the same method described in [29] and [30], to ensure homogeneity and enable a comparison with previous results, but extending the study toward other Mediterranean countries, besides Italy.

Sea-level change along the Mediterranean coast is the sum of eustatic, glaciohydro-isostatic, and tectonic factors. The first is time dependent while the latter two also vary with location, consists to sum the different components of sea level rise in the following main steps: (a) the IPCC-AR5 projections (RCP-8.5 upper limits scenarios) or Rahmstorf 2007; (b) the long term land vertical movements from geological data; (c) the glacio-hydro-isostatic movement (GIA); (d) by combining eustatic, isostatic and tectonic data projected up to 2100, we provided the expected sea-levels at 2100 for the investigated coastal areas and the expected inland extent of related marine flooding.

The choice of the study areas was decided by several different factors: (i) tectonics (stable areas only); (ii) exposure, (iii) max fetch, (iv) sedimentological material, (v) wave energy flux, (vi) bedrock and (vii) geomorphological features.

For the realization of the 16 maps (Figure 1 for geographic location, Figures 2–9) we preferred to use the global projections released by the IPCC AR5 in 2013, with the aim of comparing the new results with those previously obtained by [29] and [30], using the same parameters and models. Particularly the upper limit of the likely range of IPCC AR-5 RCP 8.5 [36] and Rahmstorf [17] scenarios (Figures 2–9 and Figure S1). The latter are in good agreement with the most recent global projections, once the uncertainties on the estimates are considered in the analysis (Table 1 and references therein).

Those values have been used in our maps to evaluate the uncertainties of the relative sea-level rise.

Most of the studied areas are well covered by EO data that were retrieved from the Internet from different agencies (Table 2) and analyzed through Geographic Information System software to obtain information on surface features and elements exposed to sea-level rise.

For the relative sea level rise case studies, we used the IPCC global mean sea level rise estimation. Indeed, the local data for the Mediterranean Sea are not accurate for several reasons. First of all, most of the global models do not consider the exchange of mass and energy across the semi-enclosed basin of the Mediterranean Sea. Therefore, we decided to not estimate the uncertainties assuming to follow the upper limit of the likely range of the RCP8.5.

Most of the studied areas are well covered by geographic information, as GIS layers, describing topographical features, morphology and exposed elements. This availability led to the generation of a geographical database and the use of GIS tools for all study phases. GIS tools enable the use of original data, thus preventing any loss of detail during the elaboration. In addition, a GIS archive allows the easy update of the resulting maps depending either on the environmental changes or on the refinement of the sea-level rise estimates.

The DTMs used for the 16 coastal areas (Tables 2 and 3) have different resolutions. The realization of the maps of (1) Fertilia, (2) Valledoria, (3) Orosei, (7) Sangro, (8) Pescara, (9) Lesina, (10) Brindisi, (12) Granelli and (14) Stagnone di Marsala were also supported by in situ surveys including low-elevation aerial views through unmanned aerial vehicle (UAV) systems and some geomorphological observations, such as the measurements of dune size, and by checking for drainage and protection systems capable of preventing or reducing the ongoing submersion (Figures 2–9; Figure S1 and Video S1).

Table 1. Global projections (cm) of sea-level rise at 2100 for different authors.

RCP	IPCC 2013 cm	IPCC 2019 cm	Kopp et al., 2016 cm	Mengel et al., 2016 cm	Horton et al., 2014 cm	Rahmstorf 2007 cm	Bamber al., 2019 cm
RCP 8.5	53–97	61–110	52–131	57–131	50–150	50–140	21–163

Table 2. Link to the websites and data (shapefiles).

Link	Project	Map Number
http://www.pcn.minambiente.it/mattm/	RITMARE	5, 6, 7, 8, 9, 10
http://www.sitr.regione.sicilia.it/?page_id=419	RITMARE	14
http://www.sardegnageoportale.it/areetematiche/modellidigitalidielevezione/	CLIMTOUR	12
http://centrodedescargas.cnig.es/CentroDescargas/buscador.do#	CLIMTOUR	1, 2, 3
https://land.copernicus.eu/	CLIMTOUR	15, 16
https://www.geoportail.gouv.fr/carte	CLIMTOUR	4, 11, 13
	CLIMTOUR	4

Table 3. A: site number; B: coastal zone; C: (digital terrain model, DTM) resolution and accuracy; D: epoch of DTM; E: IPCC projection AR5-RCP8.5 for 2100; F: IPCC projection AR5-RCP8.5 for 2050; G: Rahmstorf projection (2007); H: vertical tectonic rate mm/year; I: glacial isostatic adjustment (GIA) rate (Lambeck et al., 2011); J: relative sea-level rise for 2050, IPCC AR5-RCP8.5 scenario; K: relative sea-level rise for 2100, IPCC AR5-RCP8.5 scenario; L: sea-level rise for 2100, Rahmstorf (2007); M: relative sea-level rise for SROCC 2100; N: potential flooded area in 2100, IPCC RCP8.5; O: flooded area for 2100 in km², Rahmstorf (2007); P: exposed coastline length (km²).

A	B	C	D	E	F	G	H	I	J	K	L	M	N	O	P
Site no.	Coastal Zone	DTM Resolution and Vertical Accuracy (m)	Year	SLR Projection 2100 IPCC-8.5 (2013) (mm)	SLR Projection 2050 IPCC-8.5 -2013 (mm)	SLR Projection 2100 Rahmstorf -2007 (mm)	Vertical Tectonic Rate (mm/year)	GIA (mm/year)	Total SLR -IPCC (2013) 2050 (mm)	Total SLR- IPCC 2100 (2013) (mm)	Total SLR 2100 Rahmstorf (mm)	Total SLR-IPCC SROCC (mm)	Flooded Area 2100 IPCC-8.5 (km ²)	Flooded area 2100 Rahmstorf (2007) (km ²)	Exposed Coastline Length (km)
1	Fertilia	LiDAR 5 × 5 (±0.2)	2008	970	225	1400	0	0.57	249	1022 ±134	1452 ±134	1152.44 ±134	1.7	2.3	6.2
2	Valledoria	LiDAR 1 × 1 (±0.2)	2008	970	225	1400	0	0.57	249	1022 ±134	1452 ±134	1152.44 ±134	1	2.2	5.6
3	Orosei	LiDAR 1 × 1 (±0.2)	2008	970	225	1400	0	0.62	251	1027 ±134	1457 ±134	1157.04 ±134	1.6	3	7.6
4	Bastia	25 × 25 ±1	2010	970	225	1400	0	0.44	243	1010 ±134	1440 ±134	1139.6 ±134	21	25	29.4
5	Marina di campo	LiDAR 2 × 2 (±0.2)	2013	970	225	1400	0	0.37	239	1002 ±134	1432 ±134	1132.19 ±134	0.1	0.34	4.8
6	Tronto	LiDAR 2 × 2 (±0.2)	2008	970	225	1400	0	0.3	238	998 ±134	1428 ±134	1127.6 ±134	0.06	0.09	9.2
7	Sangro	LiDAR 2 × 2 (±0.2)	2008	970	225	1400	0	0.37	241	1004 ±134	1434 ±134	1134.04 ±134	0.08	0.13	7.2
8	Pescara	LiDAR 2 × 2 (±0.2)	2008	970	225	1400	0	0.385	241	1005 ±134	1435 ±134	1135.42 ±134	0.3	0.5	20.7
9	Lesina	2 × 2 (±0.2) (coast) 1 × 1 (±0.2) (inland)	2014	970	225	1400	See Section 3.2	0.42	243	1009 ±134	1439 ±134	1138.64 ±134	13	13	40
10	Brindisi	LiDAR 2 × 2 (±0.2)	2008	970	225	1400	0	0.44	243	1010 ±134	1440 ±134	1140.48 ±134	0.5	0.9	9.9
11	Larnaka Cyprus	25 × 25 ±1	2010	970	225	1400	0	0.21	227	989 ±134	1419 ±134	1118.9 ±134	10.3	11.6	32.7
12	Granelli	LiDAR 2 × 2 (±0.2)	2007 2008	970	225	1400	0	0.56	248	1022 ±134	1452 ±134	1151.52 ±134	5.4	6.8	14.4
13	Kerkennah	SRTM 30 × 30	2010	970	225	1400	0	0.25	234	999 ±134	1420 ±134	1122.5 ±134	82.3	109	220.1
14	Stagnone e saline di Marsala	LiDAR 2 × 2 (±0.2)	2008	970	225	1400	0	0.56	249	1022 ±134	1452 ±134	1151.52 ±134	5.4	6.9	18.5
15	Mallorca	LiDAR 5 × 5 (±0.2)	2010	970	225	1400	0	0.61	249	1025 ±134	1455 ±134	1154.9 ±134	1.3	3.7	23.1
16	Ibiza	LiDAR 5 × 5 (±0.2)	2010	970	225	1400	0	0.61	249	1025 ±134	1455 ±134	1154.9 ±134	2.9	4.2	51
	Total												148.5	192.4	407.8

2.1. Vertical Land Movements

Because the relative sea-level changes along the coastal zones also depend on the rates of the vertical land movements caused by tectonics and GIA, these geological processes were considered in the analysis, including natural ground compaction and GIA, as in Lambeck et al. [47]. To this end, we used the GIA values (Table 3) from [47] which have rates between 0.2 and 0.65 mm/year and assumed that they will be constant for the next 500 years. The Lambeck et al., 2011, is a model tested in the field of stable Mediterranean areas comparing radiocarbon ages of fossil shells sampled on cores crossing fossil lagoon areas (minimum slr error).

To account for vertical tectonics, we have used as reference the tectonic rates reported in Antonioli et al. [29] which are representative of a calibrated balance between the long-term tectonic signal (i.e., last Interglacial, [48,49]), the short-term (i.e., mid- to late Holocene, [50]; additional material of Lambeck et al. [47]) and instrumental data [22]. In addition to these, we used the upgraded Mediterranean database for the last 125 ka BP of Antonioli et al. [51], (see Section 3.1, Data). Finally, the GIA and tectonic values were included in the analysis and added to the sea-level rise projections to obtain the values of relative sea-level change expected for 2100 at each site. Vertical tectonic rates were calculated using the MIS 5.5 highstand (125 ka BP) altitude, considering the eustatic altitude in the Mediterranean Sea of 6 ± 2 m.

2.2. Digital Terrain Models

To map the sea-level rise scenarios, a data set of high-resolution topography based on light detection and ranging (LiDAR) observations produced by different agencies from 2008 to 2019 was used (Table 2). The extracted Digital Terrain Models (DTM) were obtained at variable spatial resolutions depending on the data set and in the range at about 20 cm of mean vertical resolution [52].

The details of the characteristics of the DTM are described in Table 3 and in the maps available in the online supporting material. The details regarding the link to the website from which we downloaded or requested the digital data are also described in the online supporting material. DTMs were mapped and analyzed by Global Mapper Software® (www.globalmapper.com [53]) (Version 21, Hallowell, ME, USA) to create 3D high-resolution maps of the investigated areas, on which the position of the present-day coastline and its potential position in 2100 as a result of relative sea-level rise are shown by contour lines. The DTMs with contour lines and submerged surfaces were represented using the color shaded option and exported as georeferenced images through GIS composer.

Since high-resolution LiDAR data were not available for all the investigated areas, the DTMs for Larnaka (Cyprus), Bastia (France) and Kerkennah Islands (Tunisia), were extracted from Earth Observation data retrieved at <https://land.copernicus.eu/> [54]. The technical specifications of data sources and DTMs are shown in Table 3 and discussed in Section 4.

To link the land surface to the seafloor along the coasts, the bathymetric data were obtained from GEBCO (www.gebco.net) [55] which includes regional low-resolution grids) and the European Marine Observation and Data Network (EMODnet, <http://portal.emodnet-bathymetry.eu/> [55]). Marine and terrestrial topographic data were co-registered and georeferenced into the same UTM-WGS84 (Zones 30, 31, 32 and 33, 36) reference frame, and the shoreline position was determined relative to the epoch of the surveys for each area.

The choice of study areas was dictated by several factors. The first factor was the tectonic activity; in fact, we chose only tectonically stable areas to eliminate a variable (with consequent error) in the sea-level change equation. As is known for relative sea-level change, the combined results of eustasy, glacio-hydro-isostasy and vertical tectonic motion exhibit considerable spatial variability; the first of these is time-dependent, while the latter two vary with location. As shown in Table 4, the coastal areas chosen for our research have very different exposures, maximum fetch, sedimentological material, wave energy flux, and kinds of geomorphology; our choice was precisely due to their great heterogeneity. A common characteristic of all the areas chosen was that of not having vertical tectonic movements.

Table 4. A: coastal areas chosen for our research; B, C: region and Country; D: coordinates; E: wind\wave exposure; F: maximum fetch (km); G: geological coastal material; H: annual mean energy flux (kW\m) according with [56]; I: kind of geomorphological outcrop; L: human made structures occupying the area planned to be submerged on 2100.

A	B	C	D	E	F	G	H	I	L
Coastal Site	Region	Country	Latitude and Longitude (Dedimal Degree)	Exposure Direction	Max Fetch (km)	Coastal Material	Wave Energy Flux kW/m	Geomorphology	Human-Made Structures
1 Fertilia	Sardinia	Italy	40.617889° N 8.200782° E Gr	S	505	Sand	7	Pocket beach	Fertilia town
2 Valledoria	Sardinia	Italy	40.961910° 8.840432°	NW	520	Sand ravel	4	Embayed Beach	Agricultural crops
3 Orosei	Sardinia	Italy	40.373995° 9.725289°	SW	574	Sand	1.5	Embayed Beach	Agricultural crops
4 Bastia	Corse	France	42.660470° 9.448431°	W	700	Rock	2	Barrier Lagoon	Bastia Airport
5 Marina di Campo	Island of Elba	Italy	42.748714° 10.238112°	SW	660	Sand	1,5	Pocket beach	Marina di Campo town
6 Tronto	Marche	Italy	42.896730° 13.911675°	WNW	518	Sand	1	River Delta/mainland beach	Agricultural crops
7 Sangro	Abruzzo	Italy	42.241935° 14.517749°	NW	423	Sand	1	River Delta/mainland beach	Agricultural crops
8 Pescara	Abruzzo	Italy	42.467166° 14.225779°	NW	518	Sand	1	River Delta/mainland beach	Pescara town
9 Lesina	Apulia	Italy	41.883915° 15.452643°	N	416	Sand	1.5	Coastal lake and lagoon, tombolo	Agricultural crops
10 Brindisi	Apulia	Italy	40.668235° 17.948512°	NE	688	Rock	1.5	Gently sloping rocky coast	Brindisi Airport
11 Larnaka	District of Larnaka	Cyprus	34.947170° 33.643878°	SW	403	Silt	5	Embayed Beach	Larnaka airport
12 Granelli	Sicily	Italy	36.700054° 15.024145°	SSW	770	Sand	3	Barrier Lagoon	Agricultural crops
13 Kerkennah	Governorate of Sfax	Tunisia	34.740386° 11.221183°	E	2167	Rock	2.5	Low-lying rock platform	Tourist activities
14 Marsala	Sicily	Italy	37.862205° 12.442988°	W	1605	Sand	5	Barrier Lagoon	Saltponds
15 Mallorca	Island of Mallorca	Spain	39.530120° 2.729394°	SW	637	Sand	5	Embayed Beach	Mallorca airport
16 Ibiza	Island of Ibiza	Spain	38.858203° 1.370749°	S	2730	Sand	3	Embayed Beach	Saltponds

3. Results

The 16 maps described in this section (Figures 1–9 and Figure S1, Table 3) show the expected submerged area for 2100 for the selected areas of Italy, Spain, France, Tunisia and Cyprus. For the sites investigated in the CLIMTOUR Project, 324.7 km of coast with a potential submerged area of 176.2 km² was estimated, while from the RITMARE Italian National Project and I-STORMS data set, 68.1 km of at-risk coast with possible submerged areas of 13.8 km² and 9.9 km², and 1 km² for Brindisi (I-STORMS), were estimated, respectively.

3.1. Geographic Description of the Areas at Potential Risk of Submersion

In addition to the values reported in Table 3 for the studied areas (Figure 1), we provide some information on the infrastructures located in the selected areas, such as roads and transport networks, airports, and humid protected areas, which are prone to be flooded in 2100 (Figures 2–9 and Figure S1). In situ inspections were carried out at Fertilia, Valledoria, Orosei, Sangro, Pescara, Lesina, Brindisi, Granelli and Stagnone di Marsala (Video S1).

3.1.1. Fertilia

Map 1: This zone is one of the most important coastal wetlands in Sardinia and is locally called “Il Calich”. It faces the bay of Alghero, extending from its neighbors to the town of Fertilia, and is connected to the sea by a channel (Figure 2). The coast is characterized by very well-preserved coastal dunes up to 7 m high. The presence of *Posidonia oceanica* in the marine area and the dune–lagoon system could be able to retreat in the case of sea submersion. The sector exposed to submersion risk is presently a farming area, with the exception of a large campsite located between the lagoon and the road.

3.1.2. Valledoria

Map 2: The area includes the mouth of the Coghinas River, which is interesting due to the intense agricultural cultivation of artichokes (50% of Sardinian artichoke production). It is partly located in the fluvial marine arm of the mouth of the Coghinas River, which forms a protected zone parallel to the coastline. The latter is characterized by a 5–6 m high dune system on average, with up to 12 m of elevation. Because of the absence of roads or buildings on the dune area, with the exception of a campsite, the dunes are free to retreat in case of sea-level rise (Figure S1).

3.1.3. Orosei

Map 3: The Cedrino river flows near the Orosei bay, with an estuary mouth which is closed in dry periods by a sandy shoreline which forms a marshy area—particularly rich in fauna—in the area behind it. It is the fifth longest river in Sardinia and has caused dangerous flooding in the past. The construction of a dam 20 km upstream (under Dorgali) and 5 m high embankments in the area just before the mouth prevent the river from overflowing into the plain in the depressed areas shown on the map during the floods. There are human activities and agricultural fields which are protected from the floods of the river. This high-value coastal wetland retains a subtle balance between sediments brought by the river and the rising sea, Figure 3.

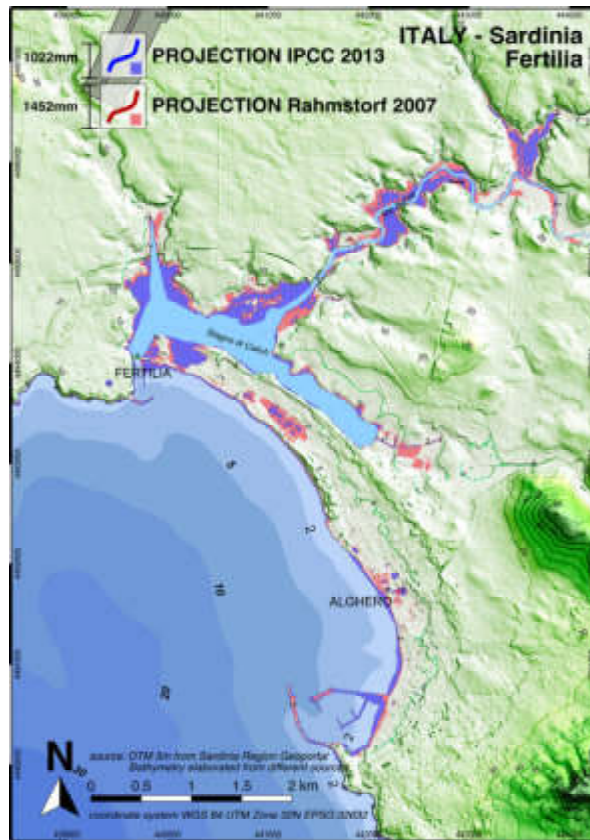


Figure 2. Map 1 Fertilia (Sardinia Italy, see also Figure 1 for location). The potential submersion area, using Rahmstorf 2007 projections are 2.3 km².

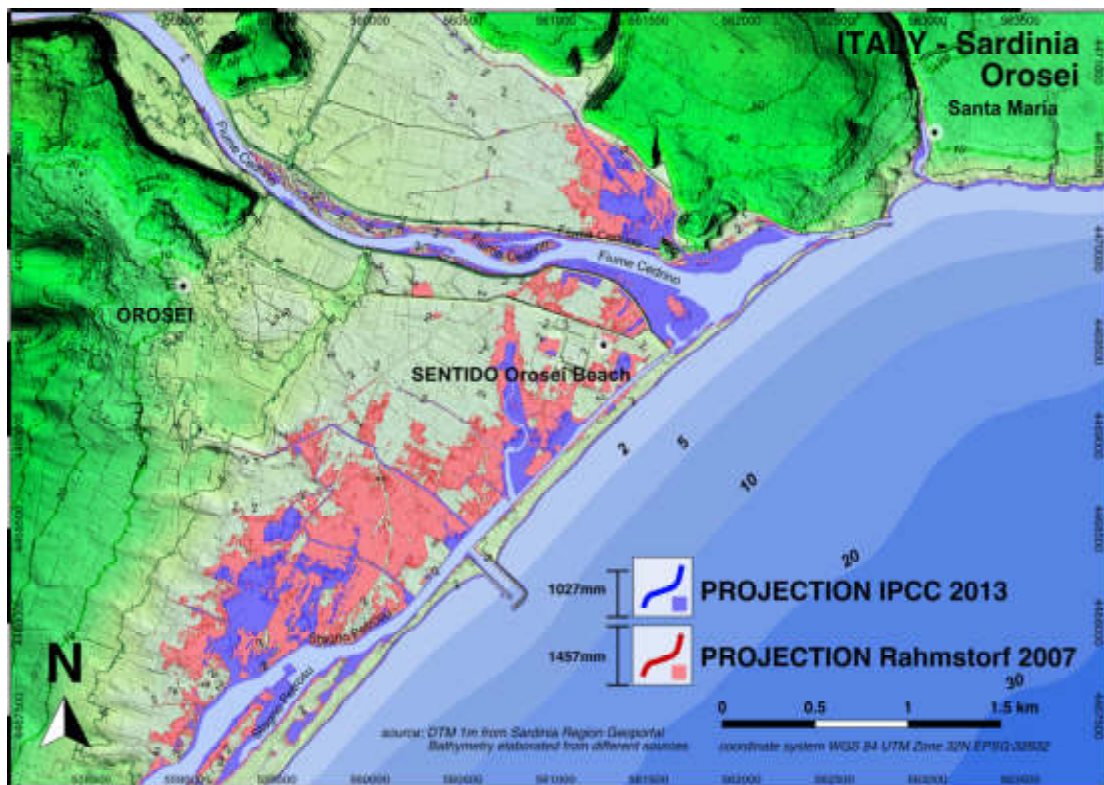


Figure 3. Map 3 Orosei (Sardinia Italy, see also Figure 1 for location). The potential submersion area, using Rahmstorf 2007 projections are 3.1 km².

3.1.4. Bastia

Map 4: The Biguglia lagoon is located south of Bastia (France) and is separated from the Tyrrhenian Sea by a sandy dune belt. It is an important wetland zone of interest that includes the largest lake in Corsica. It covers an area of 14.5 km², with a length of 11 km and a width of 2.5 km. The lagoon has two Natura 2000 protection zones and is a site of European relevance. Its large extent makes it an area of great ecological importance with high biodiversity in the Mediterranean basin due to the presence of avifauna fauna and aquatic flora. The aquatic fauna allows a large number of birds to nest, live and reproduce on the site. The external dune cord seems fairly well preserved, but there are many houses that will be exposed to sea-level rise if the dune recedes. Some rivers flow into the area and bring numerous sedimentary deposits. The area of potential submersion also falls in the northern portion of the Bastia airport (Figure S1).

3.1.5. Marina di Campo

Map 5: The Marina di Campo beach (Elba Island, Italy) is the largest of the islands (1.4 km). It is made of granite-source sand and surrounded by a thick pine forest. The dune no longer exists, and many houses in the town and the southern part of the airport are exposed to sea-level rise, Figure 4.

3.1.6. Tronto

Map 6: The Tronto River (Adriatic Sea, Italy) has a typical Apennine regime with strong floods in the rainy season (about 1500 m³/s) and in summer. The coastal dune has been eroded, except for the northern coastal portion of the river-mouth, with depressed swampy areas and farming areas at risk of submersion in 2100. On the southern side is the inhabited center of Martinsicuro, with large beaches and bridles that collect the sediments of the river that feed the beaches. Some local houses will be exposed to marine submersion in 2100.

3.1.7. Sangro

Map 7: In this area, there are small depressed zones behind the beach, mainly devoted to agriculture. Although the railway and the highway are not exposed to marine submersion as they are protected by the continuous deposit of fluvial sediments along the coasts, we note that the dunes have been eroded. The fluvial-marsh geomorphological history of the plain is described in Parlagreco et al. [57] (Figure S1).

3.1.8. Pescara

Map 8: The geomorphological evolution of the largely anthropized coastal area of Pescara is characterized by a slow progradation [58]. About 7000 years ago, the area in which the sports field of Pescara is located was a lagoonal environment. The dune system has been completely eroded. There are small depressed areas within the city, but the flow of the river sediments should counteract any submersion (Figure S1).

3.1.9. Lesina

Map 9: The Lesina Lake (a protected natural area since 1981, now part of Gargano National Park) is a brackish lagoon and an important habitat for bird species, located along the northwestern shore of the Gargano promontory (Apulia, Italy) and connected to the Adriatic Sea through three narrow artificial channels. The depth of the brackish waters does not exceed two meters. Most of the dune belts are preserved, and they do not show evidence of fast retreat, representing an important obstacle to sea-level rise. The low lands bordering the lagoonal area are devoted to agriculture and zoo technique activities. The village of Marina di Lesina may experience local instabilities due to the karst sinking into the gypsum layers, as described in Section 3.2.

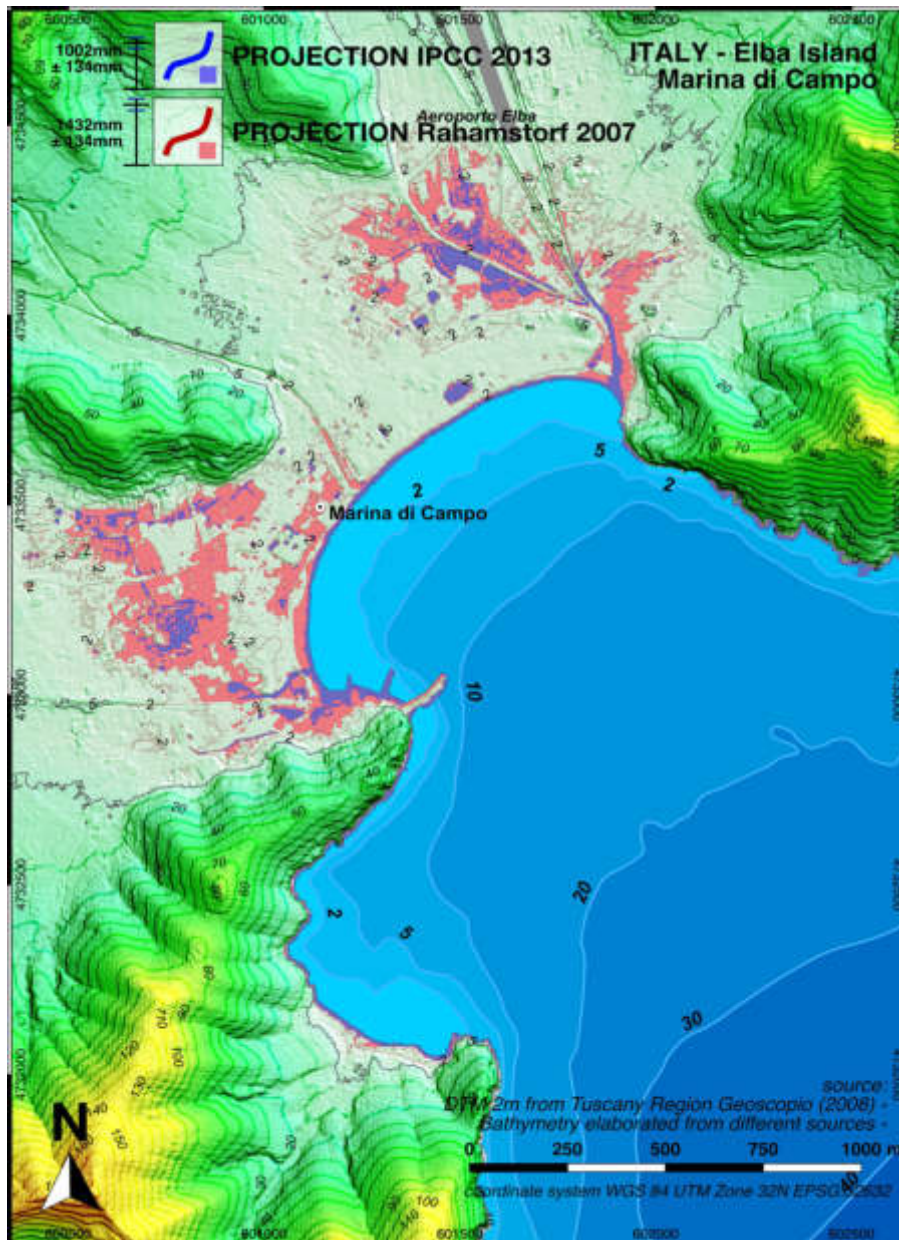


Figure 4. Map 5 Marina di Campo (Elba Island, Italy, see also Figure 1 for location). The potential submersion area, using Rahmstorf 2007 projections are 3.4 km².

3.1.10. Brindisi

Map 10: This coastal area is located in a very sensitive rocky area occupied by a peripheral part of Brindisi city, touristic settlements, archaeological and architectural sites, air–industrial facilities and the Casale airport, whose NE portion, at about 1 m above sea level, falls near the touristic harbor and connected shipyards. However, the main runway runs SE–NW at safe altitudes between 7 and 8 m (Figure S1).

3.1.11. Larnaka (Cyprus)

Map 11: The international airport area occupies the wetland area of Larnaka, with a runway placed at about 1 m above sea level. The low resolution of the map prevents any further detailed coastal hazard assessment, Figure 5.

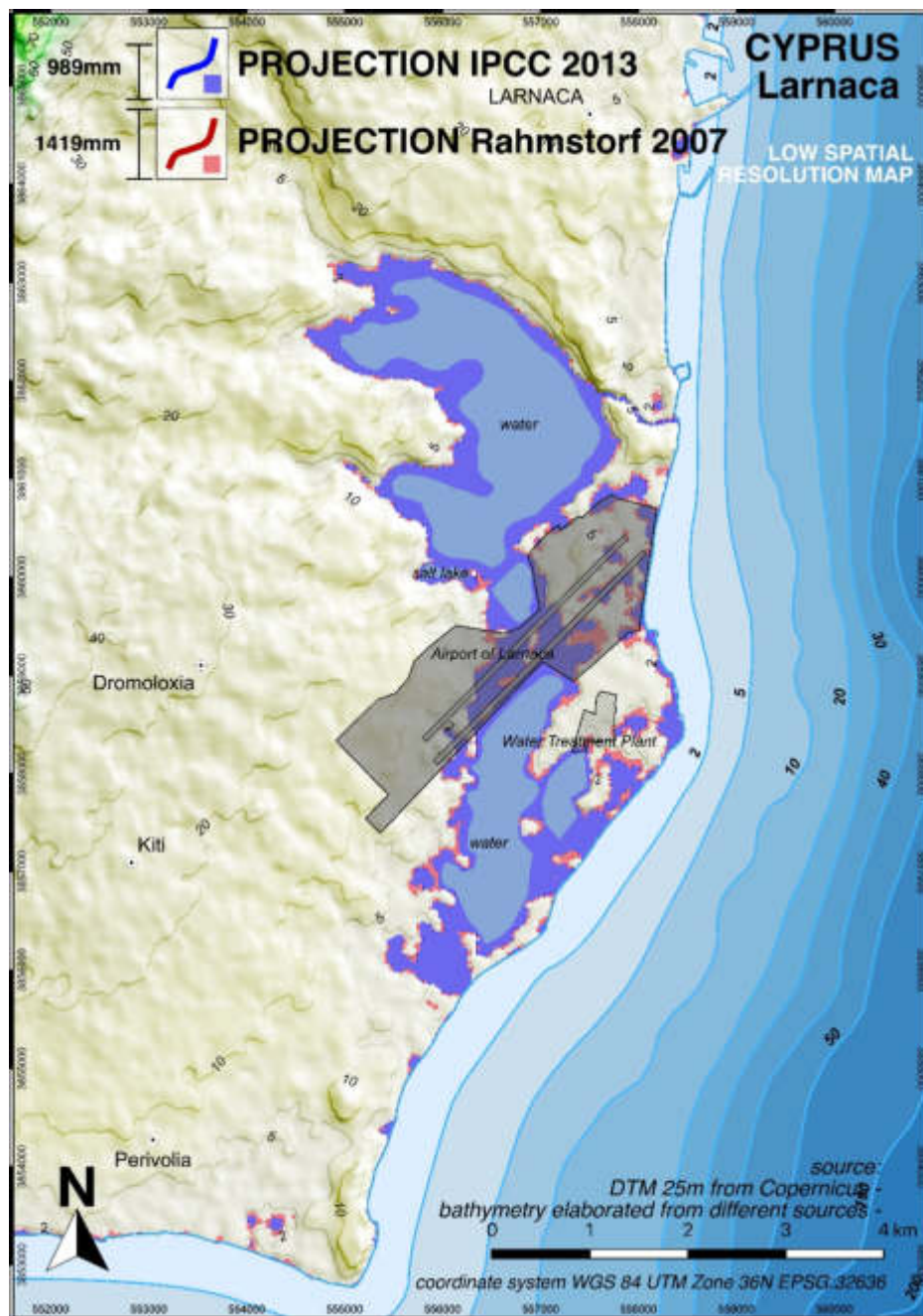


Figure 5. Map 11 Larnaka (Cyprus), see also Figure 1 for location). The potential submersion area, using Rahmstorf 2007 projections are 11.6 km².

3.1.12. Granelli (Italy)

Map 12: The Longarini lagoon is a wetland of about 0.02 km² and is known as Porto Ulisse due to its frequentation in Greek and Roman times; it is part of the wider Site of Community Importance (European Union (EU) Habitat Directive), which is one of the most important wetlands in the Mediterranean for the protection of biodiversity. It is separated from the Sicily Channel by a dune belt which is strongly urbanized and shows several paths that interrupt its continuity; thus, it does not avoid the sea flooding during extreme events and partial submersion in the next decades due to sea-level rise, Figure 6.

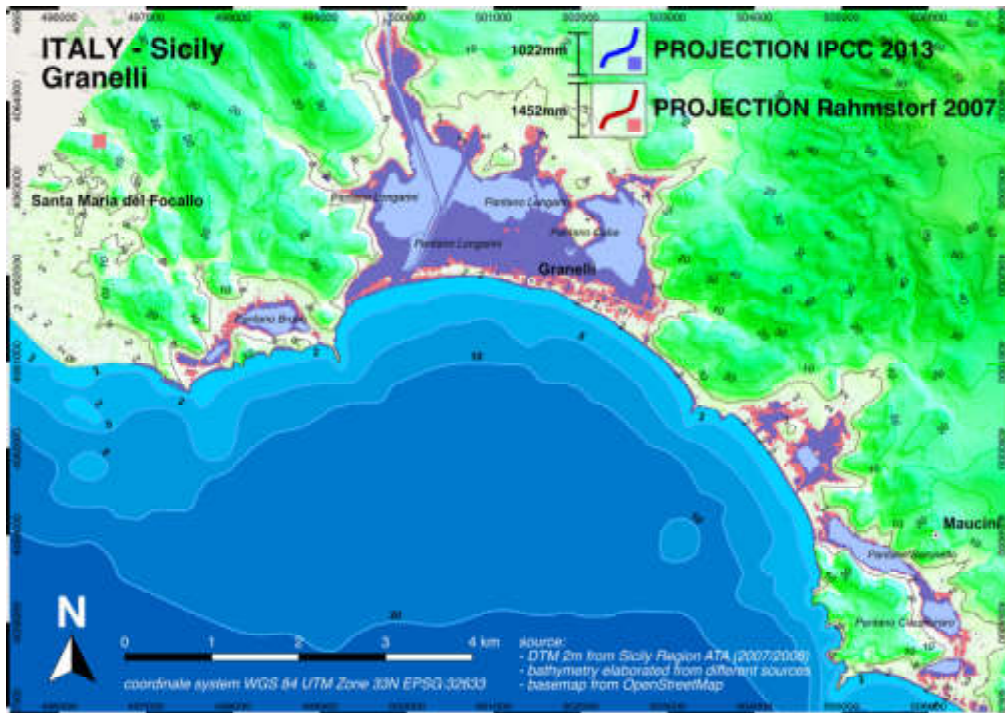


Figure 6. Map 12 Granelli (Sicily, Italy), see also Figure 1 for location). The potential submersion area, using Rahmstorf 2007 projections are 6.8 km².

3.1.13. Kerkennah

Map 13: This archipelago is located in the Gulf of Gabes (Tunisia)—a few kilometers from Sfax. It is composed of seven small and poorly inhabited rocky islands placed between 0 and 4–5 m above the sea level. In this area, the available data do not allow us to create a high-resolution DTM, preventing any reliable description of a submersion scenario. Being located close to the sea level in a stable tectonic environment, the lowest elevated coastal zones of this area are prone to be flooded by 2100, Figure 7.

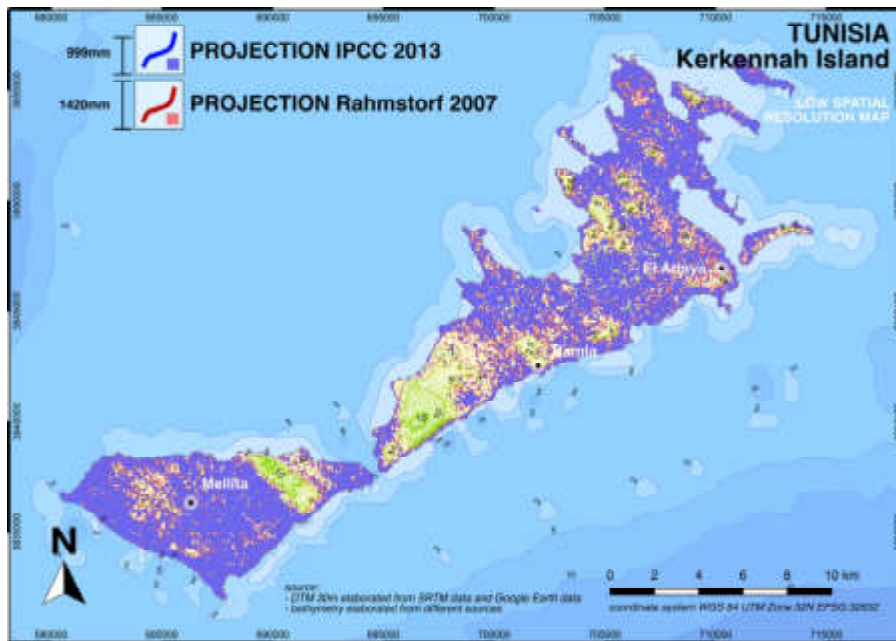


Figure 7. Map 13 Kerkennah (Tunisia), see also Figure 1 for location). The potential submersion area, using Rahmstorf 2007 projections are 109 km².

3.1.14. Stagnone e Saline di Marsala

Map 14: The Stagnone of Marsala is considered a semi-enclosed lagoon that was partially flooded by about 1 m during the Punic Age (2.3 ka BP) [41]. This area is occupied by the airport of Trapani Birgi and the nearby salt pans, with the latter being at risk of marine submersion and consequent economic loss. In particular, the runway of Birgi airport is placed between 7 and 2 m above sea level and is exposed to marine submersion during storm surges (Figure S1).

3.1.15. Mallorca

Map 15: The map shows an extremely anthropized low-elevation rocky coast, without dunes and with depressed marshy areas inside. Additionally, the north runway of the international airport is prone to marine submersion due to its low elevation above sea level, Figure 8.

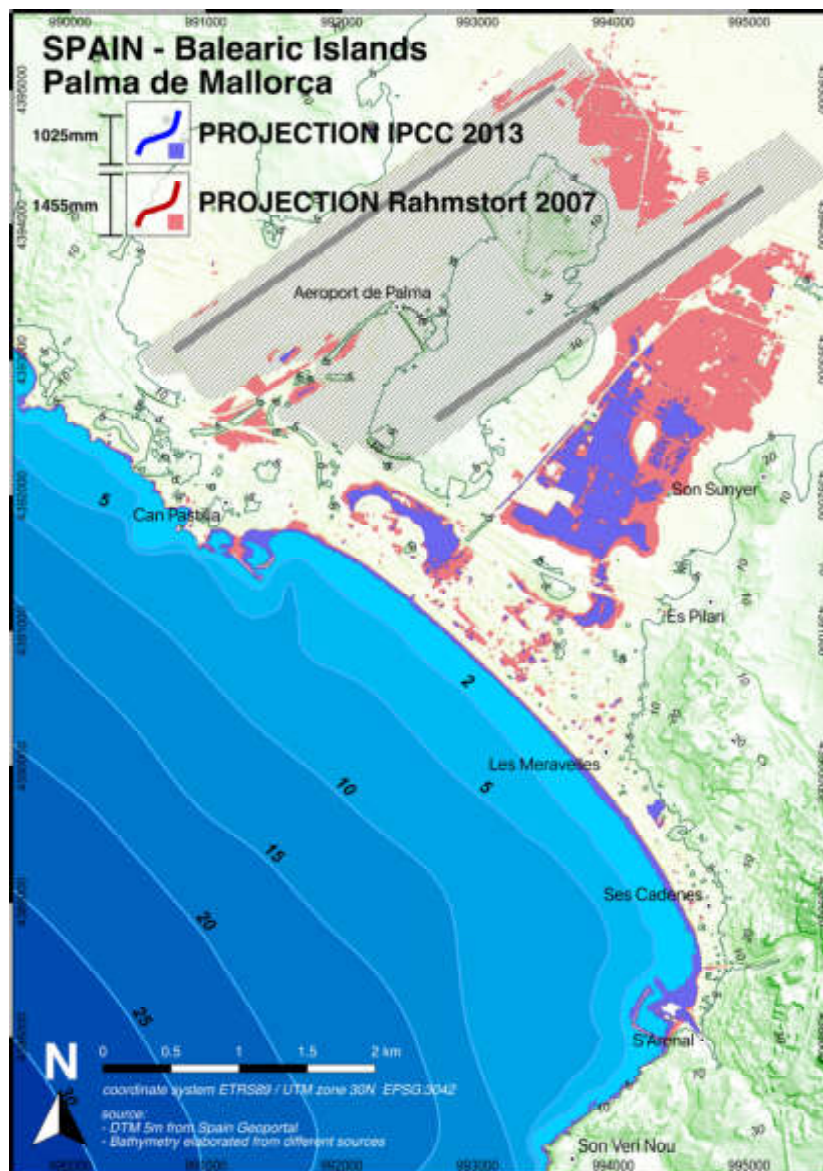


Figure 8. Map 15 Palma de Mallorca (Spain), see also Figure 1 for location). The potential submersion area, using Rahmstorf 2007 projections are 3.7 km².

3.1.16. Ibiza

Map 16: Our map highlights some depressed zones around the city of Ibiza, belonging to marshy areas. The international airport is located between 5 and 6 m of elevation above sea level and presently is not at risk of marine submersion. Conversely, some docks and parking areas of the Ibiza harbor, placed at around 1 m above sea level, are prone to sea-level rise in 2100, as well as the salt pans located east of the city (Ses Salines Natural Park). The dune that currently protects the salt marshes is active and has no obstacles to its movement; however, it is cut by a road in its northern sector, which will facilitate marine ingress over the next decades, Figure 9.

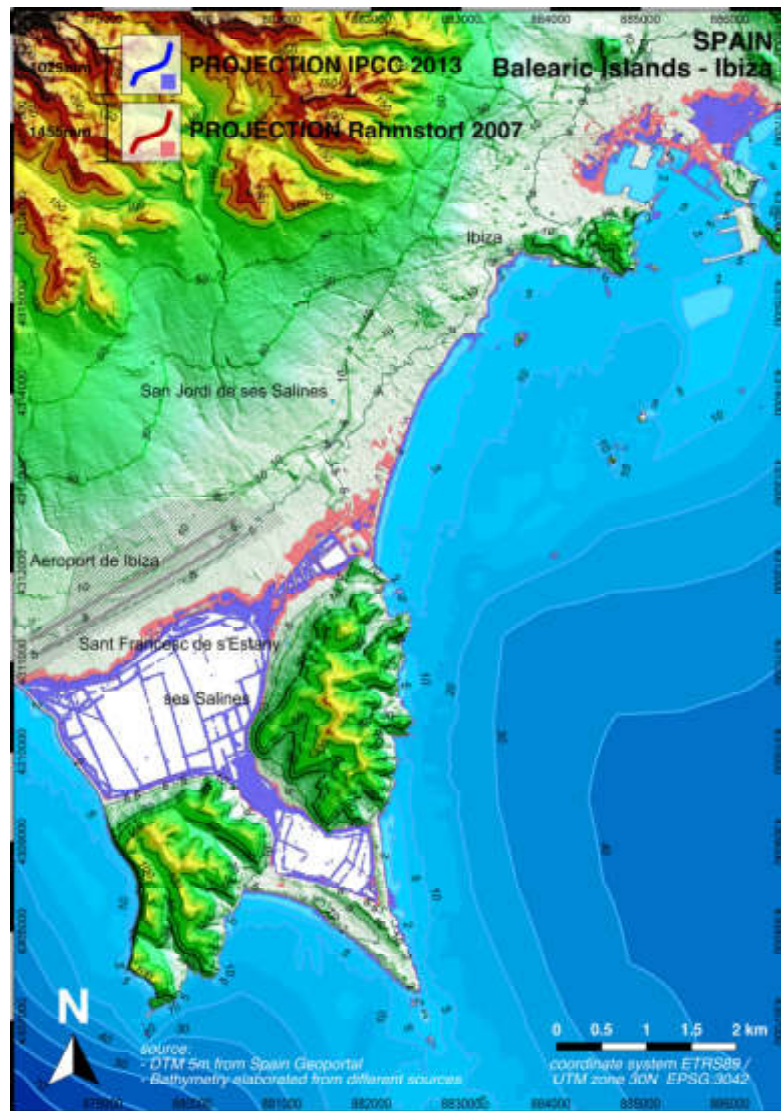


Figure 9. Map 16 Ibiza (Spain), see also Figure 1 for location). The potential submersion area, using Rahmstorf 2007 projections are 4.2 km².

3.2. New Tectonic Data

In this section, we show the vertical tectonic trends for the studied areas, which are considered tectonically stable (see Introduction and references therein). Radiocarbon data from lagoon fossil shells sampled in cores and the predicted sea-level rise for the Holocene [47] are also included in the analysis.

A recent paper for the Fertilia area [59] (for a site located 9 km from Fertilia) dated the *Lithopyllum* reef sampled into the fossil tidal notch, confirming it belongs to MIS 5.5, 125 ka BP). The tectonic stability considered for Marina di Campo (island of Elba) derives from a deposit containing *Strombus*

bubonius (now *Persitrombus latus*) found in the island of Pianosa, which is 26 km distant and at an altitude of 5 m. However, a new paper [60] was able to discuss our considerations; the radiocarbon ages of marine and brackish shells extracted from some cores, if compared with the local sea-level curve from Lambeck et al. [47], show a clear subsidence of 2–3 mm/year. If this is not due to compaction or in situ sediments, the areas of the maps highlighted by us as being at risk of possible sea submersion could be wider. There are no fossil deposits of MIS 5.5 found on the island. For the coastal area at the mouth of the Sangro river, it was possible to examine some works such as Aucelli et al. [32] and Parlagreco et al. [57] that confirmed the tectonic stability of the area. For the small depressed areas mapped around the city of Pescara, data were reported in Aucelli et al. [32] and Parlagreco et al. [58]. In this work, ENEA carried out a core in the city for the study of the lagoon's evolution down to 15 m. Apart from the first meters of soil compaction, the radiocarbon age of shells from the lagoonal environment, when compared with the sea-level curve from Lambeck et al. [47], confirm the remarkable tectonic stability.

The Lesina area is placed eastward of the mouth of the Fortore River. It is dominated by a marine terrace with pebbly deposits with the inner margin at about 25 m above sea level, attributed on a morphostratigraphic basis to a generic last Interglacial. When attributed to the MIS 5.5 last interglacial, as suggested by Mastronuzzi et al. [61], we can speculate a slow tectonic uplift. A high cliff separates it from the plain of the Fortore River; its sediments are distributed from NNW to ESE by the drift of a long shore that over time has supplied a littoral spit that has its root at Punta delle Pietre Nere and which limits Lesina Lake [62]. This area is very complex from a neotectonic point of view. A few kilometers north of the lagoon, a core carried out near to the Biferno river mouth and radiocarbon analysis on lagoon shells [63], when compared against Lambeck et al. [47], indicated a slight uplift. During the Holocene, the whole area of the plain of Fortore River underwent repeated events of slow subsidence and uplift [64,65]; these were identified thanks to the presence of the uplifted *Cladocora caespitosa* "coralligenous-like" bioconstruction of Punta di Pietre Nere (today, the top is at about 1.5 m above sea level) and by the recognized bio concretions of *Dendropoma* spp; when compared with Lambeck et al. [47], this indicates a general uplift of about 2.49 ± 0.54 mm/year [50]. In this area, the uplifting can be related to the combination of the dynamics imposed by the activity of the gypsum structure of Punta delle Pietre Nere and the regional tectonics conditioned by the structures of the Fortore River, Tremiti Islands and Gargano Promontory [66–68]. On the other hand, in the town of Lesina Marina, Caporale et al. [69] highlighted the localized subsidence of the area with rates of up to 5 mm/year due to the karst activity that produces more sinkholes in the gypsum units, while, on the basis of radiocarbon age determinations on samples derived by cores sampled near Lesina—Punta delle Pietre Nere performed by Longhitano et al. [70], a low rate of uplift may be supposed using the model of Lambeck et al. [47]. In the presence of these neotectonic differences, it was not easy to attribute tectonic rates to the map (Table 2); thus, we considered it more appropriate to make a mean of the values because there is no regional study on these local phenomena nor instrumental geodetic data. In this case, we have assumed zero tectonics, and for some small areas of the map the values could, therefore, be either in excess or too low. A few kilometers further south, just beyond the Gargano promontory, Caldara and Simone [71] published the results of a core carried out in Palude Frattarolo where the radiocarbon ages of the lagoon *Cerastoderma*, when compared with Lambeck et al. [47], indicate substantial stability [50].

The investigated area of Brindisi is characterized by outcrops of Middle–Late Pleistocene units on which the sea shaped a gently sloping rocky coast. In general, the area preserves archaeological and geomorphological evidence that indicates a very low rate of subsidence over the long term and a substantial stability during the Holocene [72–75].

The Island of Cyprus is located in a tectonically quasi-stable area (0–0.15 tectonic uplift). Galili et al. [76] reports the elevation of MIS 5.5 across the island, falling at Larnaca airport at 7 ± 0.5 m, indicating the stability of this coastal area (sea level during MIS 5.5 was 7 m higher than today in Mediterranean Sea [50]).

Regarding the coastal area of Stagnone and Saline di Marsala, there are some data [48,77] related to MIS 5.5 which indicate tectonic stability. Basso et al. [78] carried out several surveys in the Stagnone di Marsala and performed radiocarbon aging on brackish organisms such as the *Cerithium*. Findings evidenced depths of 50–70 cm and ages up to 3 and 6 ka cal BP, as if there had been considerable uplift (when compared with the curve from Lambeck et al. [47]); after extensive discussions based on the ecology of the place (personal communication with Prof. Renato Chemello), there are high chances that these environments have undergone major changes in the last 6 ka cal BP. The confirmation that this is the well-known Punic-era road (2300 year BP) which is now up to 1 m below sea level shows a paleo level of the sea of at least 1.8 m.

As regards the Mallorca and Ibiza islands, Muhs et al. [79] and the references therein testify the tectonic stability of these islands on the basis of speleothem and coral U/Th dating and amino acid analyses.

4. Discussion

The 16 maps represent an update for new areas of the flooding scenarios reported by Lambeck et al. [47] and Antonioli et al. [29]. Because some areas are not covered by high-resolution LiDAR data, three of the generated maps are affected by a lower resolution which prevented the realization of detailed submersion scenarios for the IPCC-AR5 RCP8.5 [36] and Rahmstorf [17] projections for 2100 (Table 3). Although our maps' detail shows the expected scenarios and include the contribution of the vertical land movements (due to GIA and vertical tectonics) that may accelerate the submerging process, they have been realized without taking into account the effects of the drainage systems that could keep the investigated areas dry.

Therefore, we can only speculate on the extension of the expected marine submersion in 2100 with potential related impacts on coastal morphology and infrastructures, given the chosen climatic scenarios and the estimated trend of vertical land movements.

Table 3 shows the uncertainties of the DTM obtained by LiDAR and Copernicus data (Table 2). For the latter, the RMSE (Root Mean Square Error) in terms of vertical accuracy is about ± 1 m for lowlands (less than 10% slope) as reported in the DTM v1.0 statistical validation document (<https://land.copernicus.eu/user-corner/technical-library/eu-dem-v1.0> [54]). In particular, the RMSE in Cyprus is 1.39 m, which is still too high to build up a high resolution DTM suitable to analyze in detail the sea level rise scenario for 2100. Similarly, also for Bastia (France) and Kerkennah (Tunisia) the low resolution of the spatial data prevented to realize flooding scenarios.

In particular, the relative sea level rise falls between just over a meter and the average error of Copernicus data is 1.6 m on the Z-axis, preventing the significance of the three maps of Larnaka Bastia and Kerkennah. To this issue, we compared the elevation in the DTMs from Lidar and the altitudes from Google Earth, finding a high correspondence. This comparison was also carried out on the three maps built by DTMs using Copernicus data (25×25 m), and also in this case the values are similar to the Copernicus DTM. Scientific papers concerning the vertical error of Google Earth [80–84] report that the use of new satellite since 2016, improved the quality of the data, including the Z-axis between 2.5 m and less of 1 m, with an average error of 1.6 m and even better values in flat areas.

For the Bastia area, the 1:5000 scale map (Figure 10a,b, Table 2). provides good details which are in excellent agreement with the Copernicus data (25×25 m) on the Z-axis.

The DTMs from Copernicus and SRTM (Shuttle Radar Topography Mission) compared for the vertical with Google Earth, show the uncertainty regarding the low resolution of this data: using resolution of 25×25 or 30×30 m, the slight changes in the lowlands such as dunes, bars, embankments and other features are smoothed in the pixels, thus losing information about those morphological features (natural and anthropic) that could combat the sea-level rise. Furthermore, regarding this issue, we cannot exactly assess the sea-submersion extent on these areas, but we certainly assert that they will suffer marine submersion effects in the future (on the maps of Bastia, Larnaka and Kerkennah, have been annotated with the label "LOW SPATIAL-RESOLUTION MAP").



Figure 10. (a) and (b). Bastia 1:5000 scale map, the red circle underline the altitude showing a excellent agreement with the Map 4 Bastia.

5. Conclusions

In this work, we have shown a methodology to create maps with potentially expected submersion scenarios for 2100 in 16 different selected coastal zones of the Mediterranean basin which are prone to marine submersion under the effects of relative sea-level rise. For these areas, were produced thematic maps that were based on climatic scenarios, tectonics, local geological behavior and the best available digital topography. Maps have been produced for five small coastal areas of the Adriatic Sea (Italy) and 11 areas for eight islands of the Mediterranean Sea (Sardinia, Sicily, Elba Island in Italy; Corsica in France; Cyprus; Kerkennah in Tunisia; Majorca and Ibiza in Spain). All these areas are exposed to coastal hazard due to the their low elevation above the present mean sea level, the rates of vertical land movements and their morphological features. The different characteristics affect the expected scenarios that were built for both gently sloping rocky coasts or wave-dominated coasts. The latter are often characterized by sandy mobile systems marked by the presence of extended back dune areas with swamp, lagoon or coastal lake that are particularly sensitive to sea level rise. Some areas guest natural high value sites belonging to protected areas or National Parks; some are deeply urbanized by residential or touristic settlements; others are characterized by the presence of cultural heritage, and infrastructure such as communication routes, harbors or airports.

All maps were realized with the same methodology, but only 13 out of 16 were elaborated using high-resolution data derived by LiDAR surveys. The remaining three maps (Larnaka in Cyprus; Bastia in France and Kerkennah in Tunisia) were elaborated through data freely released by the Copernicus

program with a resolution that did not allow us to map detailed scenarios. However, the land elevation of these areas was a critical factor for the expected sea-level rise for 2100.

From our analysis we estimated a potential loss of land for the above areas between about 148 km² for the IPCC-RCP8.5 scenario and 192 km² for the Rahmstorf scenario, impacting a coastline length of about 400 km, where are often located densely inhabited settlements and infrastructures. The expected scenario and the exposition of the investigated areas to coastal hazard should be considered for a cognizant management of the coastal zone.

Supplementary Materials: The following are available online at <http://www.mdpi.com/2073-4441/12/8/2173/s1>, Figure S1: Eight maps of possible submerging coastal areas in the Mediterranean Sea, Video S1: Short drone flight on some coastal plains in Italy (mp4 short film).

Author Contributions: Conceptualization: F.A., M.A., G.M., G.D.F.; Data curation: G.D.F., L.M., V.L.P., G.S. (Giovanni Scardino); Formal analysis: L.M., V.L.P., G.D.F., M.A., D.B., S.C., G.L., S.F., A.M., M.P., G.S. (Giovanni Scicchitano), G.R.; Funding acquisition: S.C., F.A., G.M., M.P.; Investigation: F.A., V.L.P., G.S. (Giovanni Scicchitano), M.A., S.C., G.L., S.F.; Methodology: F.A., M.A., G.M., G.D.F., G.S. (Giovanni Scardino) Project administration: S.C., M.P. Resources: S.C., M.P., F.A., G.M. Visualization: G.R., L.M., V.L.P., G.D.F., M.A., D.B., S.C., G.L., S.F., A.M., M.P., G.S. (Giovanni Scicchitano); Writing—original draft: F.A., M.A., G.D.F., G.L., D.B., M.P.; Writing—review and editing: M.A., F.A., S.F., G.M., G.R., G.D.F., G.S. (Giovanni Scardino). All authors have read and agreed to the published version of the manuscript.

Funding: This study has been carried out in the frame of the RITMARE Project The Italian Research for the Sea, coordinated by the Italian National Research Council and funded by the Italian Ministry of Education, University and Research (Resp. F. Antonioli, S. Carniel), the CLIMTOUR Projects (Resp. M. Petitta) and I-STORMS Project from DISTEGEO—UNIBA and Regione Puglia Civil Protection (resp. G. Mastronuzzi).

Acknowledgments: We are thankful to Egidio Trainito for the Surveys in Sardinia. Additional maps by Antonioli et al. [29] are available online at the ISPRA website at the following link: <http://portalesgi.isprambiente.it/it/news/news/scenari-di-innalzamento-del-livello-del-mare-su-alcune-aree-costiere-italiane> [85]. We are thankful to the Italian Geological Service (ISPRA), which will continue to update this database. This work was also carried out under the umbrella of the IGCP Project n. 639 “Sea-level change from minutes to millennia” (Project Leaders: S. Engelhart, G. Hoffmann, F. Yu and A. Rosentau), the savemedcoasts (www.savemedcoasts.eu) and savemedcoasts-2 (www.savemedcoasts2.eu) projects.

Conflicts of Interest: The authors declare no conflict of interest. The funders had no role in the design of the study; in the collection, analyses, or interpretation of data; in the writing of the manuscript; or in the decision to publish the results.

Abbreviations

The following abbreviations are used in the manuscript:

EO	Earth Observation
CET	Copernicus European Tourism
CLIMTOUR	Copernicus Climate Change Service: European Tourism
DTM	Digital Terrain Model
GEBCO	General Bathymetric Chart of the Oceans
GIS	Geographic Information System
MIS	Marine Isotope Stage
LiDAR	Light Detection and Ranging
IPCC AR5	Intergovernmental Panel on climate change, 2013
RCP	Representative Concentration Pathways
sRMSE	Root Mean Square Error
SRTM	Shuttle Radar Topography Mission
RITMARE	is one of the Flag Projects of the Italian Research Program funded by the Ministry of University and Research

References

1. Vermeer, M.; Rahmstorf, S. Global sea level linked to global temperature. *Proc. Natl. Acad. Sci. USA* **2009**, *106*, 21527–21532. [[CrossRef](#)] [[PubMed](#)]
2. Church, J.A.; Woodworth, P.L.; Aarup, T.; Wilson, W.S. *Understanding Sea-Level Rise and Variability*; Wiley-Blackwell: Hoboken, NJ, USA, 2010; ISBN 978-1-4443-3452-4.

3. Kemp, A.C.; Horton, B.P.; Donnelly, J.P.; Mann, M.E.; Vermeer, M.; Rahmstorf, S. Climate related sea-level variations over the past two millennia. *Proc. Natl. Acad. Sci. USA* **2011**, *108*, 11017–11022. [[CrossRef](#)] [[PubMed](#)]
4. Meyssignac, B.; Cazenave, A. Sea level: A review of present-day and recent-past changes and variability. *J. Geodyn.* **2012**, *58*, 96–109. [[CrossRef](#)]
5. Mitchum, G.T.; Nerem, R.S.; Merrifield, M.A.; Gehrels, W.R. Modern sea level changes estimates. In *Understanding Sea Level Rise and Variability*; Church, J.A., Woodworth, P.L., Aarup, T., Wilson, W.S., Eds.; Wiley: Chichester, UK, 2010; pp. 122–138.
6. Jevrejeva, S.; Moore, J.C.; Grinsted, A.; Matthews, A.P.; Spada, G. Trends and acceleration in global and regional sea levels since 1807. *Glob. Planet. Chang.* **2014**, *113*, 11–22. [[CrossRef](#)]
7. Wöppelmann, G.; Marcos, M. Coastal sea level rise in southern Europe and the nonclimate contribution of vertical land motion. *J. Geophys. Res. Ocean.* **2012**, *117*. [[CrossRef](#)]
8. Toimil, A.; Camus, P.; Losada, I.J.; Le Cozannet, G.; Nicholls, R.J.; Idier, D.; Maspataud, A. Climate change-driven coastal erosion modelling in temperate sandy beaches: Methods and uncertainty treatment. *Earth-Sci. Rev.* **2020**, *202*, 103110. [[CrossRef](#)]
9. Gornitz, V.; Couch, S.; Hartig, E.K. Impacts of sea level rise in the New York City metropolitan area. *Glob. Planet. Chang.* **2001**, *32*, 61–88. [[CrossRef](#)]
10. Walsh, K.J.E.; Betts, H.; Church, J.; Pittock, A.B.; McInnes, K.L.; Jackett, D.R.; McDougall, T.J. Using Sea Level Rise Projections for Urban Planning in Australia. *J. Coast. Res.* **2004**, *20*, 586–598. [[CrossRef](#)]
11. Miller, K.G.; Kopp, R.E.; Horton, B.P.; Browning, J.V.; Kemp, A.C. A geological perspective on sea-level rise and its impacts along the U.S. mid-Atlantic coast. *Earth's Future* **2013**, *1*, 3–18. [[CrossRef](#)]
12. Ezer, T.; Atkinson, L.P. Accelerated flooding along the U.S. East Coast: On the impact of sea-level rise, tides, storms, the Gulf Stream, and the North Atlantic Oscillations. *Earth's Future* **2014**, *2*, 362–382. [[CrossRef](#)]
13. Rehman, S.; Sahana, M.; Kumar, P.; Ahmed, R.; Sajjad, H. Assessing hazards induced vulnerability in coastal districts of India using site-specific indicators: An integrated approach. *GeoJournal* **2020**. [[CrossRef](#)]
14. Wadey, M.; Brown, S.; Nicholls, R.J.; Haigh, I. Coastal flooding in the Maldives: An assessment of historic events and their implications. *Nat. Hazards* **2017**, *89*, 131–159. [[CrossRef](#)]
15. Carreau, P.R.; Gallego, F.J. *EU25 Coastal Zone Population Estimates from the Disaggregated Population Density Data 2001*; European Commission, DG Joint Research Centre: Brussels, Belgium, 2006.
16. Church, J.A.; Clark, P.U.; Cazenave, A.; Gregory, J.M.; Jevrejeva, S.; Levermann, A.; Merrifield, M.A.; Milne, G.A.; Nerem, R.S.; Nunn, P.D.; et al. Sea-Level Rise by 2100. *Science* **2013**, *342*, 1445. [[CrossRef](#)] [[PubMed](#)]
17. Rahmstorf, S. A Semi-Empirical Approach to Projecting Future Sea-Level Rise. *Science* **2007**, *315*, 368–370. [[CrossRef](#)] [[PubMed](#)]
18. Galassi, G.; Spada, G. Sea-level rise in the Mediterranean Sea by 2050: Roles of terrestrial ice melt, steric effects and glacial isostatic adjustment. *Glob. Planet. Chang.* **2014**, *123*, 55–66. [[CrossRef](#)]
19. Kopp, R.E.; Kemp, A.C.; Bittermann, K.; Horton, B.P.; Donnelly, J.P.; Gehrels, W.R.; Hay, C.C.; Mitrovica, J.X.; Morrow, E.D.; Rahmstorf, S. Temperature-driven global sea-level variability in the Common Era. *Proc. Natl. Acad. Sci. USA* **2016**, *113*, E1434–E1441. [[CrossRef](#)]
20. Bamber, J.L.; Oppenheimer, M.; Kopp, R.E.; Aspinall, W.P.; Cooke, R.M. Ice sheet contributions to future sea-level rise from structured expert judgment. *Proc. Natl. Acad. Sci. USA* **2019**, *116*, 11195–11200. [[CrossRef](#)]
21. Zecca, A.; Chiari, L. Lower bounds to future sea-level rise. *Glob. Planet. Chang.* **2012**, *98–99*, 1–5. [[CrossRef](#)]
22. Anzidei, M.; Lambeck, K.; Antonioli, F.; Furlani, S.; Mastronuzzi, G.; Serpelloni, E.; Vannucci, G. Coastal structure, sea-level changes and vertical motion of the land in the Mediterranean. *Geol. Soc. Lond. Spec. Publ.* **2014**, *388*, 453–479. [[CrossRef](#)]
23. Reimann, L.; Vafeidis, A.T.; Brown, S.; Hinkel, J.; Tol, R.S.J. Mediterranean UNESCO World Heritage at risk from coastal flooding and erosion due to sea-level rise. *Nat. Commun.* **2018**, *9*, 1–11. [[CrossRef](#)]
24. Savemedcoasts. Available online: <http://www.savemedcoasts.eu/> (accessed on 4 April 2020).
25. Bonaldo, D.; Antonioli, F.; Archetti, R.; Bezzi, A.; Correggiari, A.; Davolio, S.; De Falco, G.; Fantini, M.; Fontolan, G.; Furlani, S.; et al. Integrating multidisciplinary instruments for assessing coastal vulnerability to erosion and sea level rise: Lessons and challenges from the Adriatic Sea, Italy. *J. Coast. Conserv.* **2019**, *23*, 19–37. [[CrossRef](#)]

26. Marcos, M.; Jordà, G.; Gomis, D.; Pérez, B. Changes in storm surges in southern Europe from a regional model under climate change scenarios. *Glob. Planet. Chang.* **2011**, *77*, 116–128. [[CrossRef](#)]
27. Lionello, P.; Conte, D.; Marzo, L.; Scarascia, L. The contrasting effect of increasing mean sea level and decreasing storminess on the maximum water level during storms along the coast of the Mediterranean Sea in the mid 21st century. *Glob. Planet. Chang.* **2017**, *151*, 80–91. [[CrossRef](#)]
28. Bonaldo, D.; Bucchignani, E.; Pomaro, A.; Ricchi, A.; Sclavo, M.; Carniel, S. Wind waves in the Adriatic Sea under a severe climate change scenario and implications for the coasts. *Int. J. Climatol.* **2020**. [[CrossRef](#)]
29. Antonioli, F.; Anzidei, M.; Amorosi, A.; Lo Presti, V.; Mastronuzzi, G.; Deiana, G.; De Falco, G.; Fontana, A.; Fontolan, G.; Lisco, S.; et al. Sea-level rise and potential drowning of the Italian coastal plains: Flooding risk scenarios for 2100. *Quat. Sci. Rev.* **2017**, *158*, 29–43. [[CrossRef](#)]
30. Marsico, A.; Lisco, S.; Presti, V.L.; Antonioli, F.; Amorosi, A.; Anzidei, M.; Deiana, G.; Falco, G.D.; Fontana, A.; Fontolan, G.; et al. Flooding scenario for four Italian coastal plains using three relative sea level rise models. *J. Maps* **2017**, *13*, 961–967. [[CrossRef](#)]
31. Aucelli, P.P.C.; Di Paola, G.; Incontri, P.; Rizzo, A.; Vilardo, G.; Benassai, G.; Buonocore, B.; Pappone, G. Coastal inundation risk assessment due to subsidence and sea level rise in a Mediterranean alluvial plain (Volturno coastal plain—Southern Italy). *Estuar. Coast. Shelf Sci.* **2017**, *198*, 597–609. [[CrossRef](#)]
32. Aucelli, P.P.C.; Di Paola, G.; Rizzo, A.; Roskopf, C.M. Present day and future scenarios of coastal erosion and flooding processes along the Italian Adriatic coast: The case of Molise region. *Environ. Earth Sci.* **2018**, *77*, 371. [[CrossRef](#)]
33. Giordano, L.; Alberico, I.; Ferraro, L.; Marsella, E.; Lirer, F.; Di Fiore, V. A new tool to promote sustainability of coastal zones. The case of Sele plain, southern Italy. *Rend. Fis. Acc. Lincei* **2013**, *24*, 113–126. [[CrossRef](#)]
34. Welcome! - IWSI-STORMS Web System. Available online: <https://iws.seastorms.eu/> (accessed on 2 May 2020).
35. Ferrarin, C.; Valentini, A.; Vodopivec, M.; Klaric, D.; Massaro, G.; Bajo, M.; Pascalis, F.D.; Fadini, A.; Ghezzi, M.; Menegon, S.; et al. Integrated sea storm management strategy: The 29 October 2018 event in the Adriatic Sea. *Nat. Hazards Earth Syst. Sci.* **2020**, *20*, 73–93. [[CrossRef](#)]
36. IPCC. *Climate Change 2013: The Physical Science Basis. Contribution of Working Group I to the Fifth Assessment Report of the Intergovernmental Panel on Climate Change*; Stocker, T.F., Qin, D., Plattner, G.-K., Tignor, M., Allen, S.K., Boschung, J., Nauels, A., Xia, Y., Bex, V., Midgley, P.M., Eds.; Cambridge University Press: Cambridge, UK; New York, NY, USA, 2013; p. 1535.
37. Aucelli, P.; Cinque, A.; Mattei, G.; Pappone, G.; Rizzo, A. Studying relative sea level change and correlative adaptation of coastal structures on submerged Roman time ruins nearby Naples (southern Italy). *Quat. Int.* **2019**, *501*, 328–348. [[CrossRef](#)]
38. Anzidei, M.; Bosman, A.; Carluccio, R.; Casalbore, D.; Caracciolo, F.D.; Esposito, A.; Nicolosi, I.; Pietrantonio, G.; Vecchio, A.; Carmisciano, C.; et al. Flooding scenarios due to land subsidence and sea-level rise: A case study for Lipari Island (Italy). *Terra Nova* **2017**, *29*, 44–51. [[CrossRef](#)]
39. Anzidei, M.; Scicchitano, G.; Tarascio, S.; de Guidi, G.; Monaco, C.; Barreca, G.; Mazza, G.; Serpelloni, E.; Vecchio, A. Coastal retreat and marine flooding scenario for 2100: A case study along the coast of Maddalena Peninsula (southeastern Sicily). *Geogr. Fis. Din. Quat.* **2019**, *41*, 5–16. [[CrossRef](#)]
40. Anzidei, M.; Doumaz, F.; Vecchio, A.; Serpelloni, E.; Pizzimenti, L.; Civico, R.; Greco, M.; Martino, G.; Enei, F. Sea Level Rise Scenario for 2100 A.D. in the Heritage Site of Pyrgi (Santa Severa, Italy). *J. Mar. Sci. Eng.* **2020**, *8*, 64. [[CrossRef](#)]
41. Ravanelli, R.; Riguzzi, F.; Anzidei, M.; Vecchio, A.; Nigro, L.; Spagnoli, F.; Crespi, M. Sea level rise scenario for 2100 A.D. for the archaeological site of Motya. *Rend. Fis. Accad. Lincei* **2019**, *30*, 747–757. [[CrossRef](#)]
42. Perini, L.; Calabrese, L.; Luciani, P.; Olivieri, M.; Galassi, G.; Spada, G. Sea-level rise along the Emilia-Romagna coast (Northern Italy) in 2100: Scenarios and impacts. *Nat. Hazards Earth Syst. Sci.* **2017**, *17*, 2271–2287. [[CrossRef](#)]
43. Rovere, A.; Furlani, S.; Benjamin, J.; Fontana, A.; Antonioli, F. MEDFLOOD project: Mediterranean Sea-level change and projection for future FLOODing. *Alp. Mediterr. Quat.* **2012**, *25*, 3–5.
44. Snoussi, M.; Ouchani, T.; Khouakhi, A.; Niang-Diop, I. Impacts of sea-level rise on the Moroccan coastal zone: Quantifying coastal erosion and flooding in the Tangier Bay. *Geomorphology* **2009**, *107*, 32–40. [[CrossRef](#)]
45. Azidane, H.; Benmohammadi, A.; Hakkou, M.; Magrane, B.; Haddout, S. A Geospatial approach for assessing the impacts of sea-level rise and flooding on the ! Kenitra coast (Morocco). *J. Mater. Environ. Sci.* **2018**, *9*, 1480–1488. [[CrossRef](#)]

46. Scardino, G.; Sabatier, F.; Scicchitano, G.; Piscitelli, A.; Milella, M.; Vecchio, A.; Anzidei, M.; Mastronuzzi, G. Sea-Level Rise and Shoreline Changes Along an Open Sandy Coast: Case Study of Gulf of Taranto, Italy. *Water* **2020**, *12*, 1414. [[CrossRef](#)]
47. Lambeck, K.; Antonioli, F.; Anzidei, M.; Ferranti, L.; Leoni, G.; Scicchitano, G.; Silenzi, S. Sea level change along the Italian coast during the Holocene and projections for the future. *Quat. Int.* **2011**, *232*, 250–257. [[CrossRef](#)]
48. Ferranti, L.; Antonioli, F.; Mauz, B.; Amorosi, A.; Dai Pra, G.; Mastronuzzi, G.; Monaco, C.; Orrù, P.; Pappalardo, M.; Radtke, U.; et al. Markers of the last interglacial sea-level high stand along the coast of Italy: Tectonic implications. *Quat. Int.* **2006**, *145–146*, 30–54. [[CrossRef](#)]
49. Ferranti, L.; Antonioli, F.; Anzidei, M.; Monaco, C.; Stocchi, P. The timescale and spatial extent of vertical tectonic motions in Italy: Insights from relative sea-level changes studies. *J. Virtual Explor.* **2010**, *36*. [[CrossRef](#)]
50. Antonioli, F.; Ferranti, L.; Fontana, A.; Amorosi, A.; Bondesan, A.; Braitenberg, C.; Dutton, A.; Fontolan, G.; Furlani, S.; Lambeck, K.; et al. Holocene relative sea-level changes and vertical movements along the Italian and Istrian coastlines. *Quat. Int.* **2009**, *206*, 102–133. [[CrossRef](#)]
51. Antonioli, F.; Ferranti, L.; Stocchi, P.; Deiana, G.; Lo Presti, V.; Furlani, S.; Marino, C.; Orru, P.; Scicchitano, G.; Trainito, E.; et al. Morphometry and elevation of the last interglacial tidal notches in tectonically stable coasts of the Mediterranean Sea. *Earth-Sci. Rev.* **2018**, *185*, 600–623. [[CrossRef](#)]
52. Cobby, D.M.; Mason, D.C.; Davenport, I.J. Image processing of airborne scanning laser altimetry data for improved river flood modelling. *ISPRS J. Photogramm. Remote Sens.* **2001**, *56*, 121–138. [[CrossRef](#)]
53. Global Mapper—All-in-One GIS Software. Available online: <https://www.bluemarblegeo.com/products/global-mapper.php> (accessed on 15 April 2020).
54. Copernicus Land Monitoring Service. Available online: <https://land.copernicus.eu/> (accessed on 15 April 2020).
55. EMODnet Bathymetry Viewing and Download Service. Available online: <https://portal.emodnet-bathymetry.eu/> (accessed on 15 April 2020).
56. Soukissian, T.; Denaxa, D.; Karathanasi, F.; Prospathopoulos, A.; Sarantakos, K.; Iona, A.; Georgantas, K.; Mavrakos, S. Marine Renewable Energy in the Mediterranean Sea: Status and Perspectives. *Energies* **2017**, *10*, 1512. [[CrossRef](#)]
57. Parlagreco, L.; Miccadei, E.; Mascioli, F.; Devoti, S.; Silenzi, S.; Antonioli, F.; Di Palo, C. Application of relative sea level rise scenarios to coastal management policy: The case of the Abruzzo Region. In Proceedings of the Geoitalia 2009, Rimini, Italy, 9–11 September 2009; p. 1.
58. Parlagreco, L.; Mascioli, F.; Miccadei, E.; Antonioli, F.; Gianolla, D.; Devoti, S.; Leoni, G.; Silenzi, S. New data on Holocene relative sea level along the Abruzzo coast (central Adriatic, Italy). *Quat. Int.* **2011**, *232*, 179–186. [[CrossRef](#)]
59. Sechi, D.; Andreucci, S.; Stevens, T.; Pascucci, V. Age and significance of late Pleistocene Lithophyllum byssoides intertidal algal ridge, NW Sardinia, Italy. *Sediment. Geol.* **2020**, *400*, 105618. [[CrossRef](#)]
60. D’Orefice, M.; Graciotti, R.; Bertini, A.; Fedi, M.; Foresi, L.M.; Ricci, M.; Toti, F. Latest Pleistocene to Holocene environmental changes in the Northern Tyrrhenian area (central Mediterranean). A case study from southern Elba Island. *Alp. Mediterr. Quat.* **2020**, *33*, 1–25.
61. Mastronuzzi, G.; Palmentola, G.; Ricchetti, G. Aspetti dell’evoluzione olocenica della costa pugliese. *Mem. Soc. Geol. Ital.* **1989**, *42*, 287–300.
62. Mastronuzzi, G.; Aringoli, D.; Aucelli, P.P.C.; Baldassarre, M.A.; Bellotti, P.; Bini, M.; Biolchi, S.; Bontempi, S.; Brandolini, P.; Chelli, A.; et al. Geomorphological map of the Italian Coast: From a descriptive to a morphodynamic approach. *Geogr. Fis. Din. Quat.* **2017**, *40*, 161–195. [[CrossRef](#)]
63. Amorosi, A.; Bracone, V.; Campo, B.; D’Amico, C.; Rossi, V.; Roskopf, C.M. A late Quaternary multiple paleovalley system from the Adriatic coastal plain (Biferno River, Southern Italy). *Geomorphology* **2016**, *254*, 146–159. [[CrossRef](#)]
64. Mastronuzzi, G.; Sansò, P. Holocene uplift rates and historical rapid sea-level changes at the Gargano promontory, Italy. *J. Quat. Sci.* **2002**, *17*, 593–606. [[CrossRef](#)]
65. Mastronuzzi, G.; Sansò, P. The role of strong earthquakes and tsunamis in the Late Holocene evolution of the Fortore River coastal plain (Apulia, Italy): A synthesis. *Geomorphology* **2012**, *138*, 89–99. [[CrossRef](#)]
66. Refice, A.; Pasquariello, G.; Bovenga, F.; Festa, V.; Acquafredda, P.; Spilotro, G. Investigating uplift in Lesina Marina (Southern Italy) with the aid of persistent scatterer SAR interferometry and in situ measurements. *Environ. Earth Sci.* **2016**, *75*, 1–13. [[CrossRef](#)]

67. Teofilo, G.; Festa, V.; Sabato, L.; Spalluto, L.; Tropeano, M. 3D modelling of the Tremiti salt diapir in the Gargano offshore (Adriatic Sea, southern Italy): Constraints on the Tremiti Structure development. *Ital. J. Geosci.* **2016**, *135*, 474–485. [[CrossRef](#)]
68. Festa, V.; Fregola, R.A.; Acquafredda, P.; De Giosa, F.; Monno, A.; Ventruti, G. The enigmatic ascent of Ca-sulphate rocks from a deep dense source layer: Evidences of hydration diapirism in the Lesina Marina area (Apulia, southern Italy). *Int. J. Earth Sci. (Geol. Rundsch.)* **2019**, *108*, 1897–1912. [[CrossRef](#)]
69. Caporale, F.; De Venuto, G.; Leandro, G.; Spilotro, G. Interventi di mitigazione del rischio da sinkholes nell'area di Lesina marina (Provincia di Foggia, Italia). *Mem. Descr. Carta Geol. D' Ital.* **2013**, *93*, 121–142.
70. Longhitano, S.G.; Della Luna, R.; Milone, A.L.; Cilumbriello, A.; Caffau, M.; Spilotro, G. The 20,000-years-long sedimentary record of the Lesina coastal system (southern Italy): From alluvial, to tidal, to wave process regime change. *Holocene* **2016**, *26*, 678–698. [[CrossRef](#)]
71. Caldara, M.; Simone, O. Coastal changes in the eastern Tavoliere Plain (Apulia, Italy) during the Late Holocene: Natural or anthropic? *Quat. Sci. Rev.* **2005**, *24*, 2137–2145. [[CrossRef](#)]
72. Mastronuzzi, G.; Sansò, P. Pleistocene sea-level changes, sapping processes and development of valley networks in the Apulia region (southern Italy). *Geomorphology* **2002**, *46*, 19–34. [[CrossRef](#)]
73. Mastronuzzi, G.; Caputo, R.; Di Bucci, D.; Fracassi, U.; Iurilli, V.; Milella, M.; Pignatelli, C.; Sansò, P.; Selleri, G. Middle-Late Pleistocene evolution of the Adriatic coastline of Southern Apulia (Italy) in response to relative sea-level changes. *Geogr. Fis. Din. Quat.* **2011**, *34*, 207–221. [[CrossRef](#)]
74. Mastronuzzi, G.; Antonioli, F.; Anzidei, M.; Auriemma, R.; Alfonso, C.; Scarano, T. Evidence of relative sea level rise along the coasts of central Apulia (Italy) during the late Holocene via maritime archaeological indicators. *Quat. Int.* **2017**, *439*, 65–78. [[CrossRef](#)]
75. Mastronuzzi, G.; Milella, M.; Piscitelli, A.; Simone, O.; Quarta, G.; Scarano, T.; Calcagnile, L.; Spada, I. Landscape analysis in Torre Guaceto area (BRindisi) aimed at the reconstruction of the late Holocene sea level curve. *Geogr. Fis. Din. Quat.* **2018**, *41*, 65–79. [[CrossRef](#)]
76. Galili, E.; Sevetoglu, M.; Salamon, A.; Zviely, D.; Mienis, H.K.; Rosen, B.; Moshkovitz, S. Late Quaternary beach deposits and archaeological relicts on the coasts of Cyprus, and the possible implications of sea-level changes and tectonics on the early populations. *Geol. Soc. Lond. Spec. Publ.* **2015**, *411*, 179–218. [[CrossRef](#)]
77. Antonioli, F.; Kershaw, S.; Renda, P.; Rust, D.; Belluomini, G.; Cerasoli, M.; Radtke, U.; Silenzi, S. Elevation of the last interglacial highstand in Sicily (Italy): A benchmark of coastal tectonics. *Quat. Int.* **2006**, *145–146*, 3–18. [[CrossRef](#)]
78. Basso, D.; Bernasconi, M.P.E.; Robba, E.M.S. Environmental evolution of the Marsala sound, Sicily, during the last 6000 years. *J. Coast. Res.* **2008**, *24*, 177–197. [[CrossRef](#)]
79. Muhs, D.R.; Simmons, K.R.; Porat, N. Uranium-series ages of fossil corals from Mallorca, Spain: The “Neotyrhenian” high stand of the Mediterranean Sea revisited. *Palaeoclimatology* **2015**, *438*, 408–424. [[CrossRef](#)]
80. Benker, S.C.; Langford, R.P.; Pavlis, T.L. Positional accuracy of the Google Earth terrain model derived from stratigraphic unconformities in the Big Bend region, Texas, USA. *Geocarto Int.* **2011**, *26*, 291–303. [[CrossRef](#)]
81. Satge, F.; Denezine, M.; Pillco, R.; Timouk, F.; Pinel, S.; Molina, J.; Garnier, J.; Seyler, F.; Bonnet, M.-P. Absolute and relative height-pixel accuracy of SRTM-GL1 over the South American Andean Plateau. *ISPRS J. Photogramm. Remote Sens.* **2016**, *121*, 157–166. [[CrossRef](#)]
82. Mulu, Y.A.; Derib, S.D. Positional Accuracy Evaluation of Google Earth in Addis Ababa, Ethiopia. *Artif. Satell.* **2019**, *54*, 43–56. [[CrossRef](#)]
83. Ragheb, A.E.; Ragab, A.F. Enhancement of Google Earth Positional Accuracy. *Int. J. Eng. Res. Technol.* **2015**, *4*, 627–630.
84. Hachani, M.A.; Ziadi, B.; Langar, H.; Sami, D.A.; Turki, S.; Aleya, L. The mapping of the *Posidonia oceanica* (L.) Delile barrier reef meadow in the southeastern Gulf of Tunis (Tunisia). *J. Afr. Earth Sci.* **2016**, *121*, 358–364. [[CrossRef](#)]
85. Scenari di Innalzamento del Livello del Mare su Alcune Aree Costiere Italiane. Available online: <http://portalesgi.isprambiente.it/it/news/news/scenari-di-innalzamento-del-livello-del-mare-su-alcune-aree-costiere-italiane> (accessed on 15 April 2020).

